Figure S1

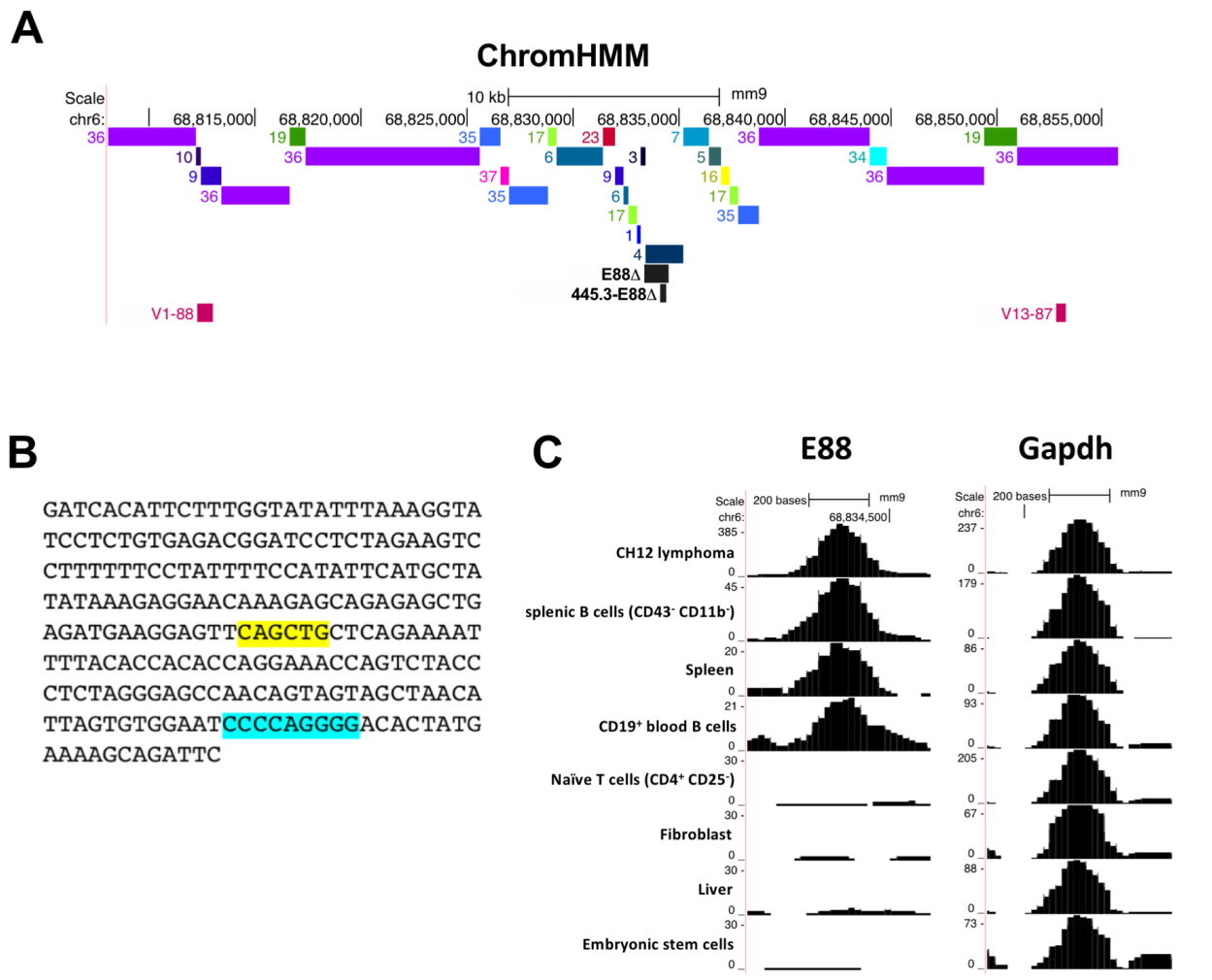

Figure S1, (related to figures 1 and 2). E88 region ChromHMM analysis, sequence and DHS specificity. (A) ChromHMM assessment of the E88 region done by (Predeus et al., 2014) in pro-B cells. Chromatin states marks: (10), H3K4me1; (19), PU.1; (23), H3K4me2; (34), Pax5; (37), E2A; (1), Mediator and H3K4me1; (9), H3K4me2 and H3K4me1; (16), H3K36me3 and H3K4me1; (17), H3ac and H3K4me1; (6), H3ac, H3K4me2 and H3K4me1; (3), DHS, E2A, H3K4me1, PU.1, and Mediator; (4), DHS, H3K4me3, H3K4me2, H3K4me1, H3ac, PU.1, Mediator, E2A, Pax5, and P300; (5), DHS, H3K4me2, H3K4me1, PU.1, and Mediator; (7), DHS, H3K4me3, H3K4me2, H3K4me1, and H3ac; (35) and (36), empty states. Indicated are the deletions made in 445.3 cells and mice (largest). (B) E88 sequence deleted in 445.3 cells with putative E2A and EBF binding sites highlighted in yellow and blue respectively. (C) DNase-seq data around the E88 area in multiple cells and tissues (Vierstra et al., 2014). An area around the GAPDH gene was used as DHS control for B cell specificity. UCSC Genome Browser views show the mapped read coverage of DNase-seq.

Figure S2

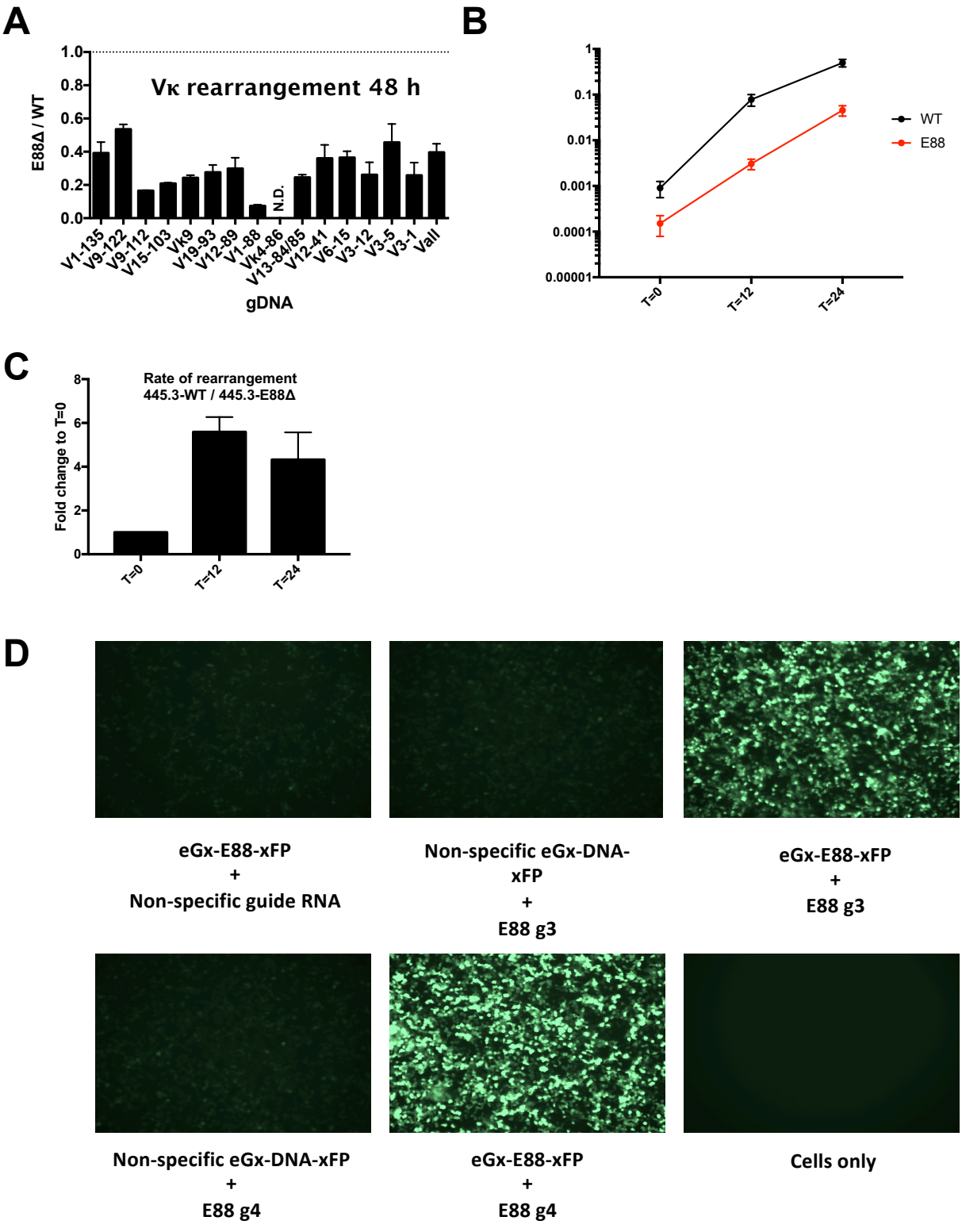
A
Vκ rearrangement 48 h
E88Δ / WT
1.0
0.8
0.6
0.4
0.2
0.0
N.D.
V1-135
V9-122
V9-112
V15-103
Vk9
V19-93
V12-89
V1-88
Vk4-86
V13-84/85
V12-41
V6-15
V3-12
V3-5
V3-1
Vall
gDNA
B
1
0.1
0.01
0.001
0.0001
0.00001
T=0
T=12
T=24
WT
E88
C
Rate of rearrangement
445.3-WT / 445.3-E88Δ
Fold change to T=0
8
6
4
2
0
T=0
T=12
T=24
D
eGx-E88-xFP
+
Non-specific guide RNA
Non-specific eGx-DNA-xFP
+
E88 g3
eGx-E88-xFP
+
E88 g3
Non-specific eGx-DNA-xFP
+
E88 g4
eGx-E88-xFP
+
E88 g4
Cells only

Figure S2, (related to figures 2 and 3). Effects of E88Δ in Vκ rearrangement pattern and early kinetics in 445.3 cell lines. (A) Quantification of Vκ rearrangement on gDNA by qPCR (TaqMan) with specific V gene primers in 445.3-WT or 445.3-E88Δ cells at 48 hours after STI571 stimulation. Data is normalized with a loading gDNA control (Eu) and is expressed as the ratio of E88Δ / WT. (B) Quantification of Vκ rearrangement on RNA by qPCR in 445.3-WT or 445.3-E88Δ cells at 0, 12, and 24 hours after STI571 stimulation with the Vall primer, which gives an estimated measure of the total rearrangement. Data is expressed relative to GAPDH. (C) Relative rate of total rearrangement (Vall) shown as the ratio of WT / E88Δ normalized to t=0 at the indicated time points. Data in A, B and C is representative of at least three independent experiments ± SEM. N.D.= not detected for WT or E88Δ. (D) Assessment of sgRNAs specificity and efficiency. pX330-E88g3 and pX330-E88g4 plasmids were tested for efficiency of targeting of the E88 region using the eGx-E88-xFP reporter plasmid (Mashiko et al., 2013). GFP expression indicates that the sgRNA-guided CAS9 endonuclease targets the DNA inserted in the multiple cloning site (MCS) in the middle of the GFP gene. Indicated plasmids were cotransfected in 239T cells and assessed for GFP expression 48 hours post-transfection. (Top left) eGx-E88-xFP plasmid cotransfected with a pX330 plasmid expressing a gRNA not specific for the E88 region. The eGx-control.DNA-xFP plasmid, containing a control DNA fragment that is not targeted by E88g3 or E88g4, cotransfected with pX330-E88g3 (top center) or the pX330-E88g4 (left bottom) plasmids. The eGx-E88-xFP plasmid cotransfected with pX330-E88g3 (top right) or pX330-E88g4 (middle bottom) plasmids. Control cells that were not transfected (right bottom). Pictures are from one of the two experiments performed.

Figure S3

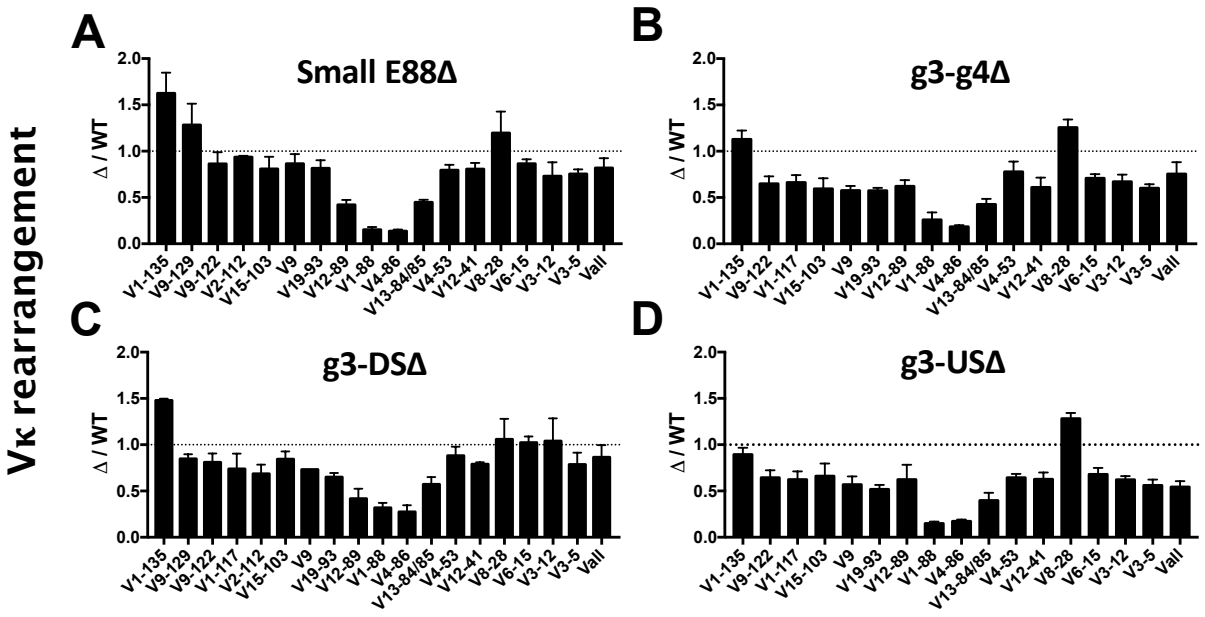

Figure S3, (related to figure 3). E88 enhancer regulates Vκ gene utilization in mice. E88 was deleted in mice using CRISPR/Cas9 editing system. Schematic of the different sized E88 deletions in mice is shown in Figure 3A. DS=downstream, US=upstream. (A-D) BM-derived $CD19^{+}$ cells were purified, and RNA was harvested. Vκ rearrangement was assessed by qPCR for specific individual Vκ genes for all the mouse lines. Data was normalized with GAPDH and expressed as E88Δ / WT ratio ± SEM. Two to five mice 6-10 weeks of age were used for each experiment. Data was collected from at least three independent biological samples.

Figure S4

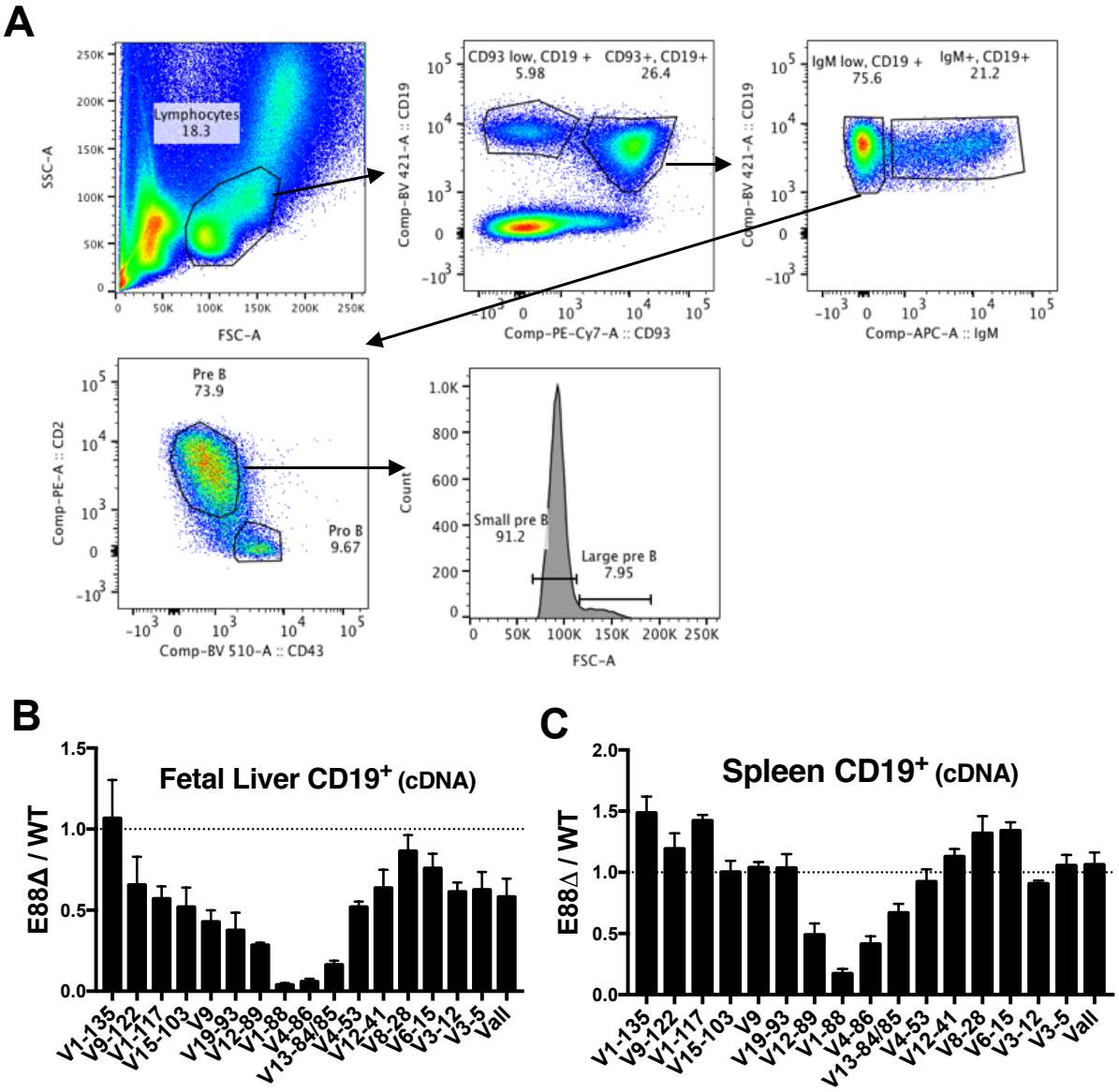

Figure S4, (related to figure 4). Sorting scheme for pro-B and small pre-B cells and Vκ rearrangement in fetal liver cells and spleen. CD19$^+$ cells were isolated from BM-cells from WT and E88Δ mice using CD19-conjugated MACS beads. (A) CD19$^+$ cells were stained with antibodies against CD19, CD93, CD2, CD43 and IgM. Sorted pro-B cells (CD19$^+$ CD93$^+$, IgM$^-$, CD2$^-$, CD43$^+$) and small pre-B cells (CD19$^+$ CD93$^+$, IgM$^-$, CD2$^+$, CD43$^-$) were used to isolate RNA or gDNA for qPCR analysis or deep sequencing. Pre-B cells were separated as large or small based on the forward scatter (FSC). (B, C) Vκ rearrangement in fetal liver and spleen CD19$^+$ cells. Isolated CD19$^+$ cells from fetal liver of embryos at day 17 of gestation or spleens from 6-10 week-old mice were used to extract RNA. Quantification of Vκ gene rearrangement was done by qPCR with specific primers for the indicated Vκ genes. Data is shown as the ratio of E88Δ / WT and was normalized to GAPDH expression. Data is representative of at least three independent experiments ± SEM.

Figure S5

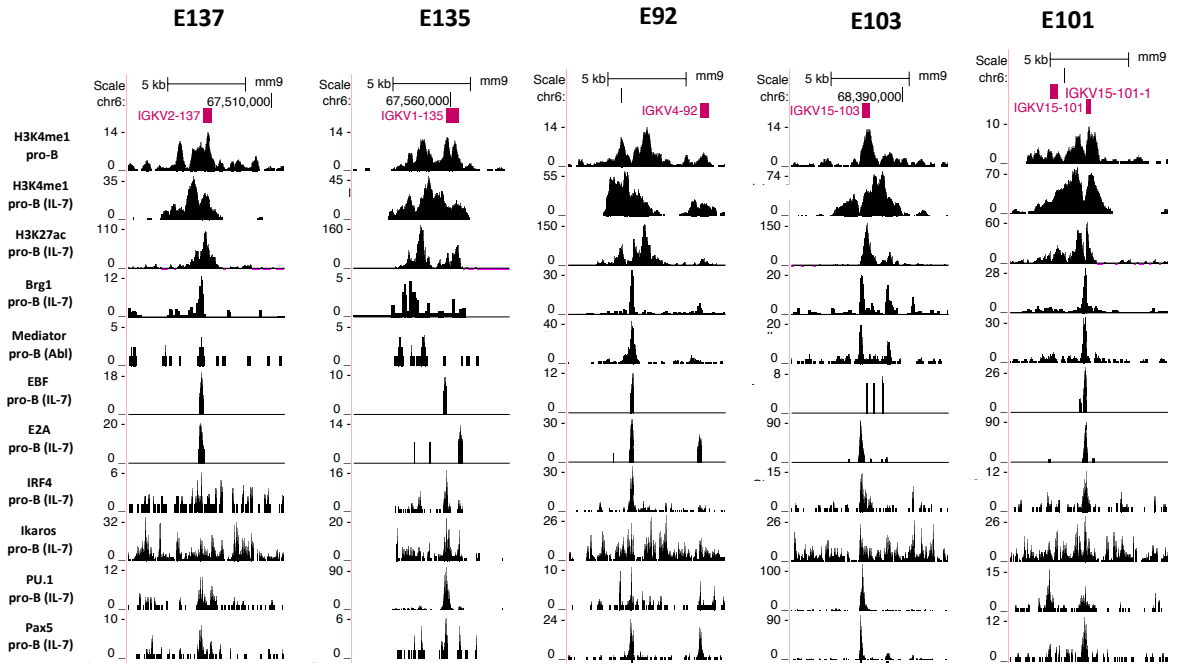

Figure S5, (related to figures 6 and 7). Chromatin profile and transcription factor binding for other identified enhancer-like regions. UCSC Genome Browser presentation of ChIP-seq datasets for the indicated putative enhancer regions. H3K4me1 (non-IL7-cultured RAG$^{-/-}$ pro-B cells and IL7-cultured RAG$^{-/-}$ pro-B cells), Mediator (v-Abl transformed pro-B cell line), and the following ChIP-seq using IL7-cultured RAG$^{-/-}$ pro-B cells: H3K27ac, Brg1, EBF, E2A, IRF4, PU.1, and PAX5. E92 has ~89% sequence similarity with E88 over ~ 650 kb. Note that the scales are different for the ChIP-seq tracks for the different enhancers.

Table S1. Primers, probes, and oligonucleotides (related to Figures 1, 2, 3, 4, 6, 7, S1, S2, and S3)

Table S2. ChIP-seq and RNA-seq datasets (related to Figures 1, 2, 3, 4, and S4)

Feature	B-cell	Accession	Analysis and notes
H3K4me1	Pro-B	GSM1897403	
H3K4me1	Pre-B	GSM2084579	
H3K4me1	Pro-B + IL7	GSM546527	
Brg1	Pro-B + IL7	GSM1635413	
H3K27ac	Pro-B + IL7	GSM1463433	
E2A	Pro-B + IL7	GSM546523	
YY1	Pro-B	GSM1897387	
Mediator1	Abl pro-B cell line	GSM1038263	
CTCF	Pro-B	GSM1156665	
CTCF	Pro-B + IL7	GSM987805	
CTCF	Pre-B	GSM2973687 GSM2973689	
Rad21	Pro-B	GSM1156667	
p300	Pro-B	GSM987808	
Pax5	Pro-B + IL7	GSM932924	
EBF	Pro-B + IL7	GSM546524	
PU.1	Pro-B + IL7	GSM1296533	
IRF4	Pro-B + IL7	GSM1296534	
ATAC-seq	ALP	GSM1635403 GSM1635399	Provided as a BedGraph
ATAC-seq	BLP	GSM1635404 GSM1635400	Provided as a BedGraph
ATAC-seq	Pro-B + IL7	GSM1635407 GSM1635409	Provided as a BedGraph
Ikaros	Pro-B + IL7	GSM1296535	
RNA-seq 1	Pro-B WT	pending	
RNA-seq 2	Pro-B E88Δ	pending	
RNA-seq 3	Pro-B WT	pending	
RNA-seq 4	Pro-B E88Δ	pending	
RNA-seq 5	445.3-WT	pending	
RNA-seq 6	445.3-WT	pending	
RNA-seq 7	445.3-WT	pending	
RNA-seq 8	445.3-WT-Cre	pending	
RNA-seq 9	445.3-E88Δ	pending	
RNA-seq 10	445.3-E88Δ	pending	
RNA-seq 11	445.3-E88Δ	pending	

Table S3. DESeq2 analysis of 4C data (related to Figures 6 and 7)